

Wood-Derived Composites with High Performance for Thermal Management Applications

Dong Wang, Yu Zhang, Mengfei Zhang, Yang Wang,* Ting Li, Tianxi Liu, Mingqing Chen, and Weifu Dong*



Cite This: *Biomacromolecules* 2021, 22, 4228–4236



Read Online

ACCESS |



Metrics & More



Article Recommendations



Supporting Information

ABSTRACT: Fabricating advanced polymer composites with remarkable mechanical and thermal conductivity performances is desirable for developing advanced devices and equipment. In this study, a novel strategy to prepare anisotropic wood-based scaffolds with a naturally aligned microchannel structure from balsa wood is demonstrated. The wood microchannels were coated with polydopamine-surface-modified small graphene oxide (PGO) nanosheets via assembly. The highly aligned porous microstructures, with thin wood cell walls and large voids along the cellulose microchannels, allow polymers to enter, resulting in the fabrication of the wood–polymer nanocomposite. The tensile stiffness and strength of the resulting nanocomposite reach 8.10 GPa and 90.3 MPa with a toughness of 5.0 MJ m⁻³. The thermal conductivity of the nanocomposite is improved significantly by coating a PGO layer onto the wood scaffolds. The nanocomposite exhibits not only ultrahigh thermal conductivity (in-plane about 5.5 W m⁻¹ K⁻¹ and through-plane about 2.1 W m⁻¹ K⁻¹) but also satisfactory electrical insulation (volume resistivity of about 10¹⁵ Ω·cm). Therefore, the results provide a strategy to fabricate thermal management materials with excellent mechanical properties.



INTRODUCTION

As the modern electronic devices are integrated and miniaturized, effective heat dissipation has become a critical issue in high-power electronic equipment and thermal management materials (TMMs).^{1–10} Consequently, considerable efforts have been devoted to developing high-efficiency TMMs. Polymers, particularly epoxies, with advantages of low cost, light weight, corrosion resistance, and high processing performance have applicability in the field of TMMs. Generally, due to phonon scattering caused by numerous structural defects, most polymer materials show poor capacity of heat transmission (0.1–0.5 W m⁻¹ K⁻¹), which makes them unfavorable for TMMs.^{11–16} So far, much efforts have been made to improve the thermal conductivity of epoxy by incorporating ceramic fillers (e.g., BN, Al₂O₃, MgO, and AlN).^{17–19} However, high ceramic filler loading is required to achieve improved thermal performance, leading to the loss of the processing and mechanical properties of polymers. Generally, carbon- and metal-based materials are more effective in improving the thermal performance of composites because of their high intrinsic thermal conductivity, but simultaneously their electrical conductivity will limit their application in some electronic fields.^{20,21} Therefore, it is still difficult to achieve high thermal conductivity enhancement while maintaining the electrical insulation and mechanical properties. It is believed that effective interfacial interaction, intrinsic thermal conductivity of the filler, and filler orientation are the main factors for high thermal conductivity enhancement.¹⁵ However, the ability to control the filler orientation

and interfacial interactions simultaneously to achieve highly thermal conductive yet electrically insulating polymer composites with excellent mechanical properties remains a challenge.

In recent years, natural structural materials have displayed impressive performance and provided a new opportunity for the development of high-performance polymer composites. For example, wood is a sustainable structural material with lightweight design, which can be readily processed, has low cost, shows relatively excellent mechanical performance, and is used in building and furniture construction.^{22–25} Generally, wood is a natural material with a hierarchical structure comprising of cellulose hollow fibrils embedded in hemicelluloses and lignin.²⁶ The hollow microfibrils offer tubular channels for the transportation of water and ions during transportation and metabolism.^{27,28} The peculiar structure and the strong interface interaction provide outstanding performance. In particular, removing lignin and hemicellulose from wood could provide a unique anisotropic and porous structure that is easy for modification. The porous structure can be further impregnated with polymers to fabricate wood-based materials for engineering applications.^{29–36} The colored lignin

Received: June 19, 2021

Published: September 9, 2021



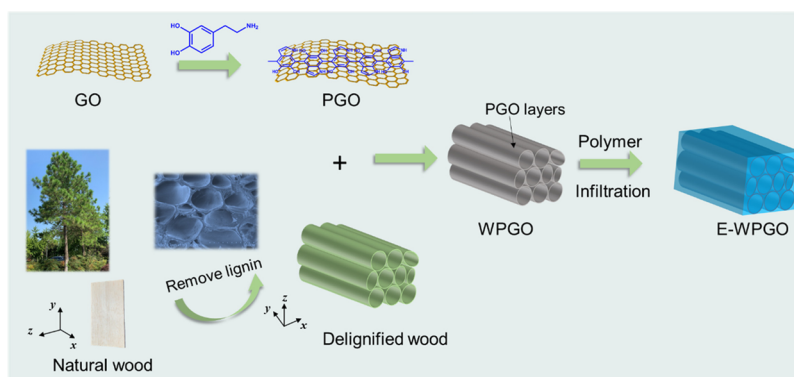


Figure 1. Schematic of the fabrication procedure of E-WPGO nanocomposites.

in the cell wall is removed by chemical treatments and mixed with index-matching epoxy resin to achieve high light transmittance. However, the hydrophobic polymers show poor compatibility with the polar wood scaffolds. This usually leads to weak interface interactions between wood scaffolds and resin, which negatively affects the performance.³⁷ Delignified wood, with unique orderly microstructures, is an ideal candidate for fabrication of transfer channels. When heated by a radiative heating source, the layered structure of aligned delignified wood nanochannels can transport heat along the cellulose alignment direction.³⁸ However, the delignified wood scaffold exhibits thermally insulating properties with a low thermal conductivity of $\sim 0.03 \text{ W m}^{-1} \text{ K}^{-1}$ in the transverse direction and $\sim 0.06 \text{ W m}^{-1} \text{ K}^{-1}$ along the cellulose alignment direction.³⁸

Polydopamine (PDA) is a well-known biomacromolecule. Dopamine can be oxidized and it spontaneously self-polymerizes under alkaline conditions and forms a PDA coating on all types of material surfaces.³⁹ Dopamine can also readily induce reduction and functionalization of graphene oxide.⁴⁰ In our previous studies, we found that PDA could act as an insulating layer to significantly reduce the transmission of electrons between nanofillers and improve the dielectric properties.^{41,42} The PDA layer was able to greatly improve miscibility between the nanofiller and the epoxy.⁴³ In this study, based on the naturally aligned microchannels, high thermally conductive wood-derived composites were prepared for thermal management. The natural wood was first processed via chemical treatment to obtain a delignified wood template with aligned microchannels. PDA was applied to modified graphene oxide (GO) under a weak alkaline condition. The PDA-surface-modified GO (PGO) was then assembled on the aligned microchannels in natural wood through interaction between PDA and cellulose, leading to the formation of heat-transfer channels. The composites were manufactured through immersion of wood-based scaffolds in the epoxy resin. Simultaneously, PDA enhances interfacial interactions between the wood scaffolds and the polymer, which successfully endows the composite with excellent tensile properties and fracture toughness.

EXPERIMENTAL SECTION

Materials. Flake graphite, sulfuric acid (98%, H_2SO_4), dopamine (98%), and hydrogen peroxide (H_2O_2 , 30%) were purchased from Sigma-Aldrich. Balsa wood was used in this study.

Delignification of Wood Samples. Balsa wood was prepared with different sizes. The delignification process of wood was carried out in an acetate buffer solution (pH 4.6) with NaClO_2 (1 wt %). The

mixture was then kept at $80 \text{ }^\circ\text{C}$ to remove lignin. The samples were stored at $30 \text{ }^\circ\text{C}$ and 50% humidity for 24 h, and they were not dried or soaked before delignification. When the wood samples were completely bleached after 72 h, the bleached wood was washed with deionized water at least for three times to remove the residues. Then the delignified wood (DW) was freeze-dried for further use. About 1.2% lignin was left in the DW according to Hu's report.³⁰

Preparation of PGO. GO was synthesized from graphite flakes as reported previously.⁴⁴ In order to synthesize relatively small GO sheets, the prepared GO should be treated by repeated oxidation.⁴⁵ The PGO was prepared according to our previous studies.⁴⁶ GO (0.1 g) and dopamine (0.05 g) were added into a Tris buffer solution (200 mL, pH 8.5) under stirring at $60 \text{ }^\circ\text{C}$ for 24 h. Afterward, the product was centrifuged and washed with deionized water. Then, the obtained PGO was freeze-dried for 24 h.

Modification of the DW Scaffold. A PGO suspension (0.5 wt %) was prepared by strong stirring for 30 min followed by sonication for 10 min. The unmodified and DW scaffold was immersed in PGO while performing a low vacuum treatment (0.3 bars for 2 h). Then the samples were washed with deionized water for three times, and then the obtained samples (WPGO) were freeze-dried. For comparison, the PGO suspension was changed with the GO suspension (0.5 wt %), and the corresponding sample (WGO) was also prepared using the same procedure.

Fabrication of Wood–Polymer Nanocomposites. The wood scaffold after coated with PGO was immersed in the epoxy resin to prepare composites. The product was cured at $80 \text{ }^\circ\text{C}$ for 3 h and then at $120 \text{ }^\circ\text{C}$ for 3 h, which was coded as “E-WPGO.” For comparison, DW and WGO were immersed in the epoxy resin to prepare composites (denoted as E-W and E-WGO) using the same procedure, respectively.

Characterization. An atomic force microscope (AFM, Multimode 8) was used to measure the thickness of GO. A scanning electron microscope (SEM, Hitachi S-4800) was used to observe the morphology of the scaffolds and nanocomposites. A Fourier transform infrared spectrometer (FTIR, Nicolet 6700, Thermo Scientific, USA) was used to determine the functional groups. The cure reaction of epoxy composites was carried out using a differential scanning calorimeter (DSC 8000, PerkinElmer) under a nitrogen atmosphere at a heating rate of $10 \text{ }^\circ\text{C min}^{-1}$. Thermal gravimetric analysis (TGA) was performed using a PerkinElmer instrument with a heating rate of $10 \text{ }^\circ\text{C min}^{-1}$ under N_2 . The mechanical properties of epoxy composites were measured using an Instron 5967 with a crosshead speed of 2 mm/min. Thermal conductivity was measured using a Netzsch LFA 467 HyperFlash. The volume resistance was tested using a ZC36 high resistance meter (Shanghai Sixth Meter Factory Co., Ltd).

RESULTS AND DISCUSSION

The design concept of thermally conductive wood composites was inspired by the photosynthesis of trees. Figure 1 illustrates the schematic diagram of the fabrication of E-WPGO

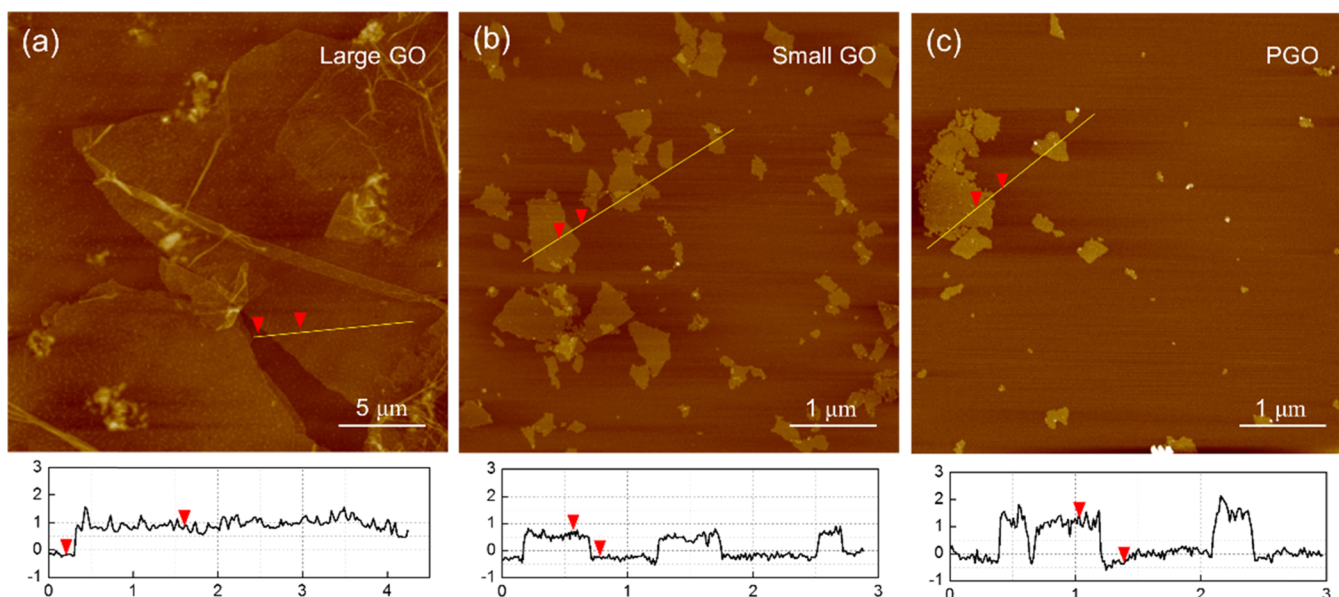


Figure 2. AFM topography images of (a) large GO, (b) small GO, and (c) PGO nanosheets and the corresponding curves of the nanosheet surface scale.

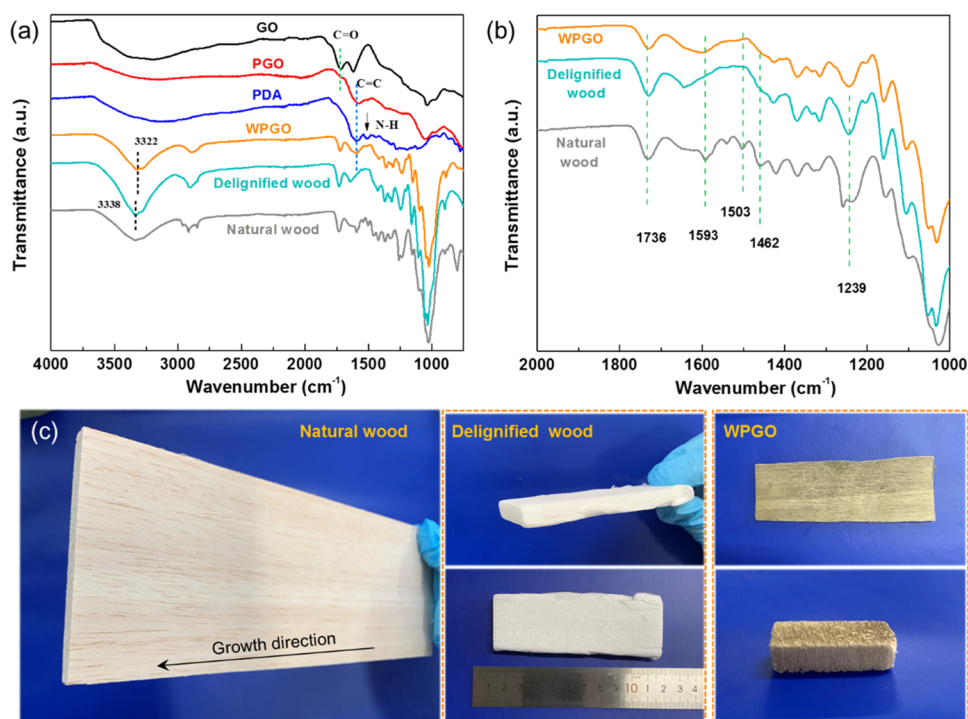


Figure 3. (a,b) FTIR spectra of GO, PGO, PDA, WPGO, natural wood, and DW. (c) Photos of a board of natural wood, DW, and WPGO, respectively.

nanocomposites. DW was impregnated with PGO to fabricate WPGO scaffolds. As shown in Figure S1, the amount of PGO adsorbed in WPGO increased gradually in a period 90 min, and when the adsorption time increased to 2 h, the amount of PGO reached ~ 23 wt %. By dipping epoxy resin into the modified wood scaffold, it is easy to prepare wood-based composite materials.

Repeated oxidation was performed to cut GO into small nanosheets. The morphologies of GO nanosheets were investigated by AFM. As shown in Figure 2a,b, GO nanosheets exhibit a kind of a wrinkled surface. The thicknesses of the two

types of GO nanosheets are quite similar (1.02–1.06 nm). The lateral size of large GO is about 20 μm, while the lateral size of small GO is less than 1 μm. The small GO was subsequently reduced with PDA. The lateral size of PGO did not change due to this process, while the thickness of PGO increased to 1.79 nm, illustrating the coating of PDA on the surface of GO.

More characteristics of the samples were obtained by FTIR analysis. GO shows the characteristic peaks at 978 and 1622 cm⁻¹ (C=C vibrations), 1034 cm⁻¹ (C–O–C), and 1717 cm⁻¹ (C=O). PGO shows a new peak at 1587 cm⁻¹ due to PDA on GO nanosheets (Figure 3a).⁴⁷ Furthermore, the

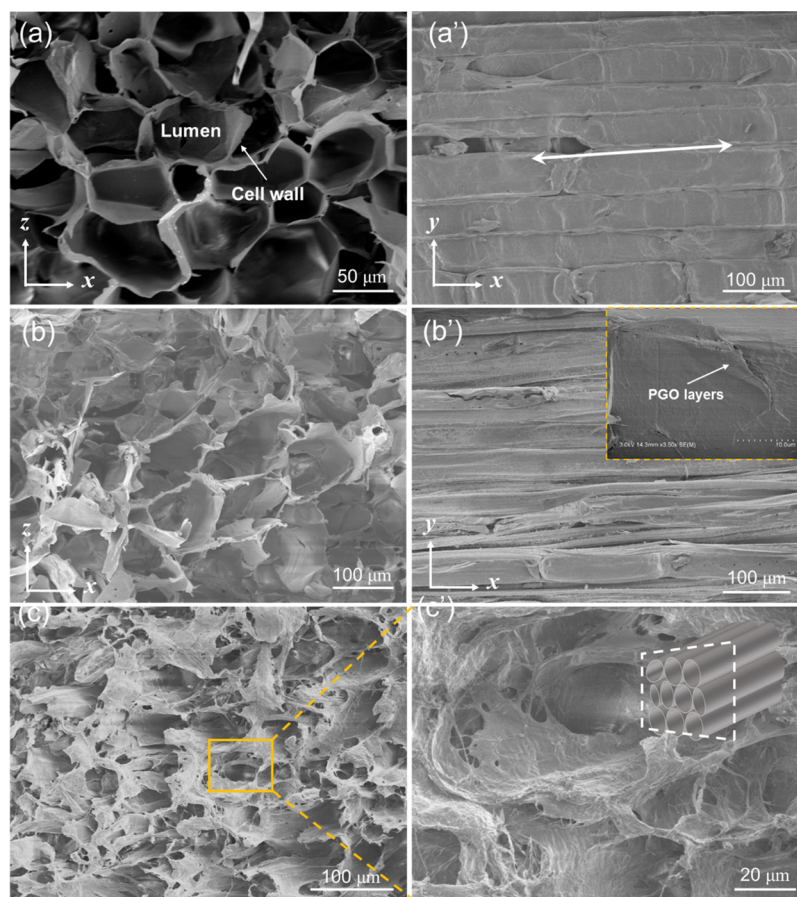


Figure 4. (a,b) Top-view, (a',b') longitudinal direction, and (c,c') oblique-view SEM images of DW and WPGO, respectively. The inset picture in (b') is the high-magnification SEM image of WPGO.

disappearance of C–O–C stretching of PGO was due to the reduction of GO by the PDA coating. For natural wood, the peaks at 3334 and 2925 cm^{-1} are ascribed to the stretching vibration of –OH and C–H, respectively. The peak at 1239 cm^{-1} is caused by C–O of the guaiacyl ring. The color of natural wood is pale yellow due to light absorption of lignin (Figure 3c). When most lignin was removed, the DW appears white. As shown in Figure 3b, the peaks of lignin at 1593, 1503, and 1462 cm^{-1} disappear.⁴⁸ For WPGO, the absorption bands at 1589 and 1513 cm^{-1} are assigned to the aromatic C=C stretching vibration and the N–H shearing vibration of an aromatic secondary amine in PDA,^{49,50} indicating that DW was successfully covered by PGO nanosheets.

The morphologies of natural wood, DW, and WPGO were investigated by SEM. After lignin removal, the lumen holes (well-defined honeycomb-like structures), which are composed of hollow fiber cells along parallel growth ($\sim 50 \mu\text{m}$), remain on the DW scaffold (Figure 4a). From the longitudinal direction SEM image (Figure 4a'), long microchannels along the growth direction are observed. It is known that wood microchannels can form a continuous porous transportation network as a water conveyance unit in trees. After the functionalization by PGO nanosheets, WPGO exhibits a dark coating as shown in Figure 3c. Figure 4b,c shows that WPGO still retains a similar honeycomb structure. In high-magnification micrographs (Figure 4b',c'), a rougher surface of WPGO is observed in microchannels due to interactions between PGO and wood cellulose, indicating the presence of the PGO layer.

In practical applications, polymer composites should show high strength and low brittleness; therefore, it is important to evaluate the mechanical properties of E-WPGO nanocomposites. The stress–strain curves of natural wood, pure epoxy, E-W, and E-WPGO nanocomposites were recorded, and the results are shown in Figure 5. A pure epoxy resin shows a tensile strength of 40.6 MPa with low elongation at break (4.30%), and the modulus of pure epoxy is 1.25 GPa. The tensile strength and modulus of E-W|| (applied stress parallel to the wood channel direction) are 56.7 MPa and 2.76 GPa, respectively, which exceed those of epoxy and natural wood. This is mainly attributed to the strengthening effect from the longitudinally oriented cellulose nanofiber structure. The E-WPGO|| nanocomposite shows superior mechanical properties with a fracture strength and modulus up to 90.3 MPa and 8.10 GPa, which are 2.2 and 6.5 times higher than those of epoxy, respectively. Moreover, E-WPGO|| shows improved toughness (5.0 MJ m^{-3})—about 5 and 7 times higher than that of pure epoxy and E-W, respectively. The tensile strength of E-WGO|| and E-WGO \perp is 57.1 and 24.2 MPa, respectively, which is lower than that of E-WPGO. The PDA layer effectively enhances the interactions of WPGO scaffolds and epoxy, which promotes the load transfer and energy dissipation among the WPGO scaffolds and epoxy and hence tremendously improves the mechanical properties of E-WPGO. The abundant catechol groups of PDA on the WPGO scaffolds play a key role in significantly enhancing the interfacial interactions. Although the presence of amine harder molecules could become proton-acceptor, C–O–C and OH

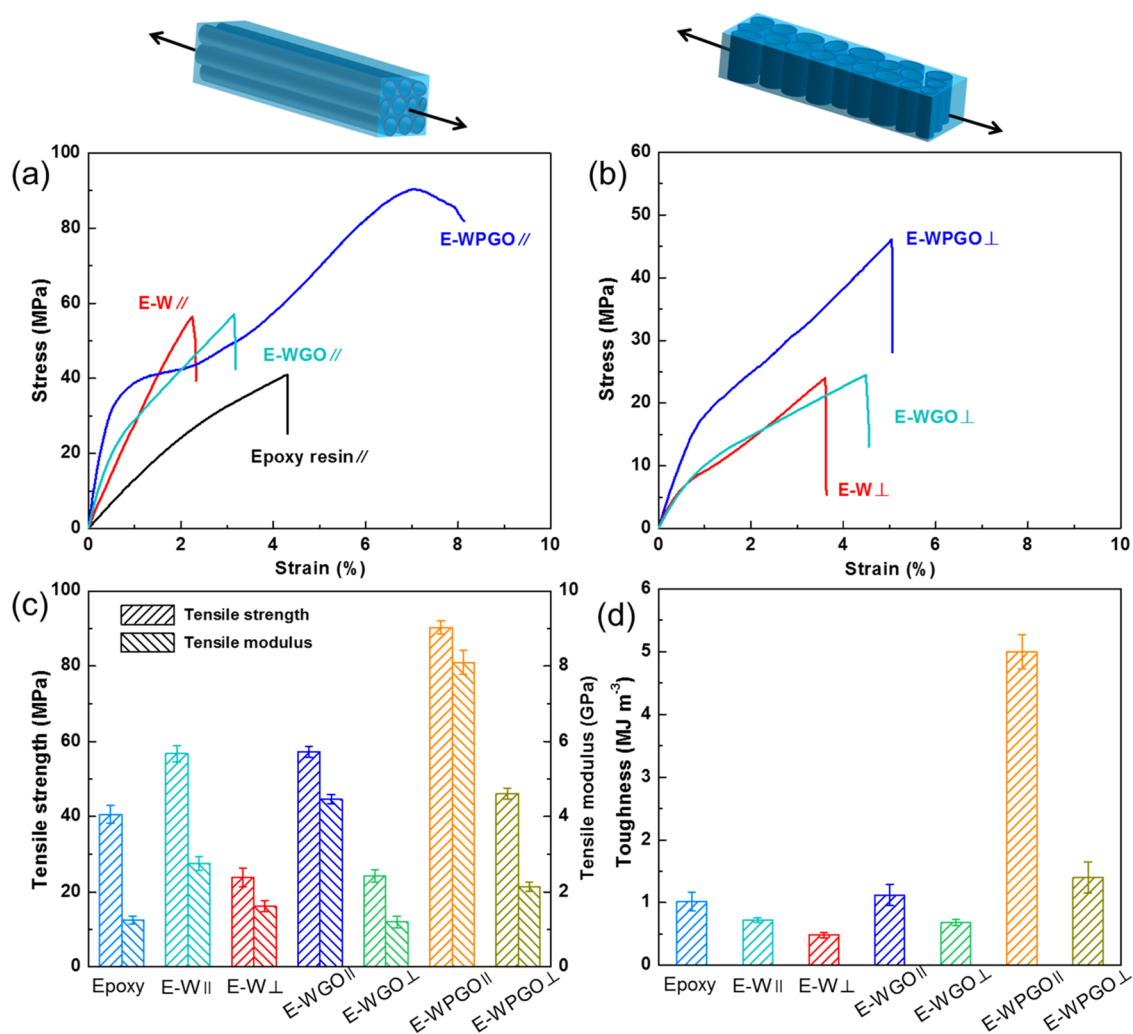


Figure 5. (a,b) Stress–strain curves of the pure epoxy, natural wood, E-W, E-WGO, and E-WPGO nanocomposites. (c) Tensile strength and tensile modulus of pure epoxy, E-W, E-WGO, and E-WPGO nanocomposites. (d) Toughness of pure epoxy, E-W, E-WGO, and E-WPGO nanocomposites (calculated by integrating the area under the stress–strain curves).

groups of epoxy could also form hydrogen bonds with PDA. More importantly, the possibility of interfacial covalent interactions cannot be completely neglected. For example, the $-\text{NH}_2$ of the curing agent could be connected to the PDA on scaffolds through Michael addition or a Schiff base reaction. The $-\text{NH}_2$ and $-\text{NH}-$ of PDA could also react with epoxy.^{51–53} As shown in Figure S2, the peak observed in the uncured epoxy resin occurs at 915 cm^{-1} due to the epoxide group. After the cure reaction, the epoxide band of the cured epoxy resin reduced, indicating the reaction of epoxide groups. As it can be clearly seen, compared with the cured epoxy resin, the epoxide characteristic peak at 915 cm^{-1} of the E-WPGO composite disappeared; also, a broad absorption of $-\text{OH}$ and $-\text{NH}-$ near 3340 cm^{-1} decreased compared to that of WPGO. A DSC analysis was performed to further study the cure reaction (Figure S3). These results suggest that the reaction between epoxide groups and amine groups of PDA. The unique mesostructured cellulose could also lead to anisotropic, mechanical properties in different directions. The tensile strength and modulus of E-W \perp are only 24.0 MPa and 0.16 GPa, respectively. Compared with E-W \perp , the tensile strength of E-WPGO \perp reaches 46.06 MPa, and with enhanced

toughness of 1.40 MJ m^{-3} , it is about three times higher than that of E-WPGO \perp .

Figure 6 shows the cryofracture surface of E-W and E-WPGO, respectively. The epoxy infiltration process completely

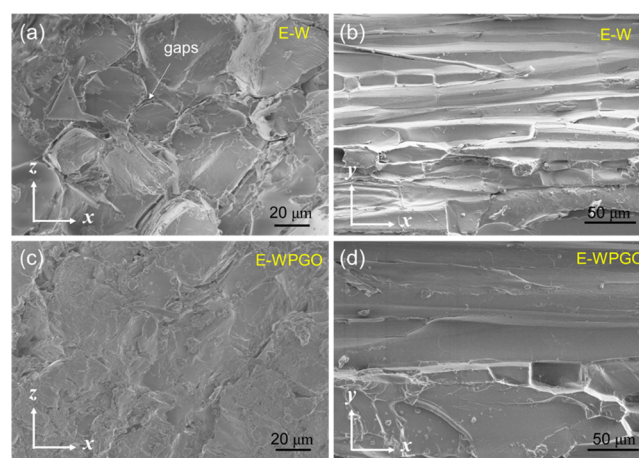


Figure 6. SEM micrographs of (a,b) E-W and (c,d) E-WPGO, respectively.

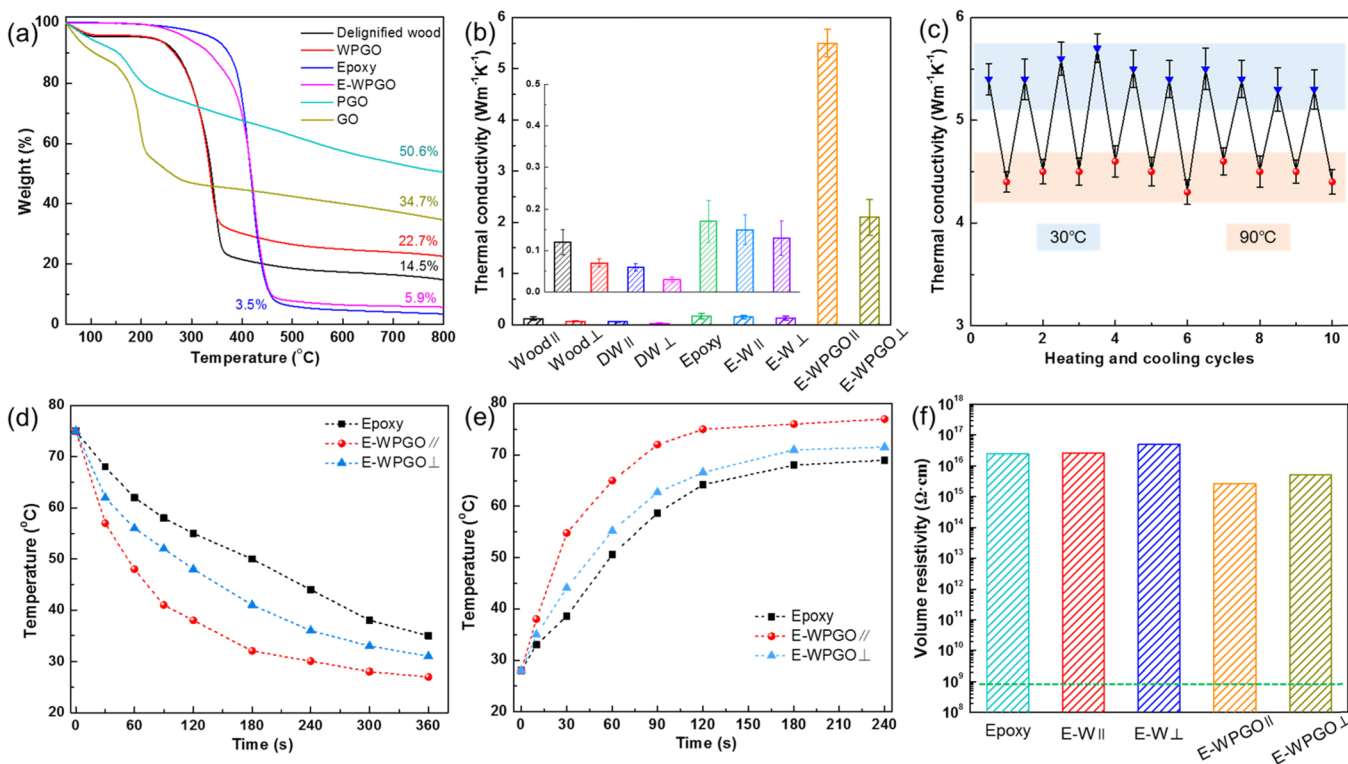


Figure 7. (a) TGA curves of DW, GO, PGO, WPGO, epoxy resin, and E-WPGO nanocomposites. (b) Thermal conductivity of wood, DW, epoxy, E-W, and E-WPGO. (c) Thermal cycling stability of E-WPGO under multiple heating and cooling cycles. (d) Cooling and (e) heating curves of the samples. (f) Volume electrical resistivity of epoxy, E-W, and E-WPGO nanocomposites. Note that || and \perp of composites denote parallel and perpendicular wood channel directions, respectively.

filled the cell lumen with epoxy resin without destroying the wood microchannels. The wooden microchannels form the frame of cellular networks, while epoxy is arranged neatly in rectangular cellular chambers. The parallel tubes could be observed with a layer spacing as shown in the E-W nanocomposite (Figure 6a,b), indicating a low interfacial interaction. What is remarkably different between the E-W and E-WPGO nanocomposites is the interfacial adhesion between wood scaffolds and the polymer, as observed in Figure 6c,d. The interface between the WPGO/epoxy cell wall and the epoxy-rich lumen region appears well integrated, which indicates favorable interfacial interaction between the epoxy resin and the WPGO cell wall. As mentioned above, because the interface regulated the hydrogen and covalent bonds, remarkable interface adhesion is observed, which is conducive to enhancing the mechanical performance of the E-WPGO nanocomposite. In order to further investigate the interfacial interaction of composites, the tensile fracture surfaces of E-WGO and E-WPGO are shown in Figure S4. The obvious gaps, pull out, and debonding between WGO and epoxy are observed, indicating a weak interfacial performance. However, E-WPGO showed lessened gaps and even seamless interfaces between WPGO and epoxy, demonstrating the enhanced interfacial compatibility. The hydrogen bonding and chemical cross-linking could be the driving forces for interfacial solubilization.

As shown in Figure 7a, GO exhibits two degradation stages. The first weight loss below 100 °C can be attributed to the removal of residual aqueous solution. The second stage takes place at 150–200 °C corresponding to the pyrolysis of the oxygen group and carbon oxidation.⁴⁶ The thermal weight loss of PGO is lower than that of GO due to high thermal stability.

The PGO enhances the thermal stability of DW. The loading of PGO is determined to be 22.7 wt % for WPGO. The content of WPGO is \sim 12.5 wt % in the E-WPGO nanocomposite calculated by the mass loss at 800 °C. Figure 7b shows the thermal conductivity of the E-WPGO nanocomposites. Thermal conductivities of the pure epoxy resin and the E-W nanocomposite were also provided for comparison. The thermal conductivity of the epoxy resin is only $0.17 \text{ W m}^{-1} \text{ K}^{-1}$. Natural wood and DW possess low thermal conductivities of 0.12 and $0.06 \text{ W m}^{-1} \text{ K}^{-1}$ in parallel wood channel directions, respectively. Moreover, the E-W nanocomposite exhibits reduced thermal conductivity values ($0.15 \text{ W m}^{-1} \text{ K}^{-1}$ for E-W|| and $0.13 \text{ W m}^{-1} \text{ K}^{-1}$ for E-W \perp). The decrease in the thermal conductivity is mainly due to the low interfacial interaction between wood scaffolds and epoxy, as observed in Figure 6a, and the corresponding increase in the thermal conduction resistance. In comparison, the thermal conductivity of the E-WPGO \perp nanocomposite can reach $2.1 \text{ W m}^{-1} \text{ K}^{-1}$, which is nearly 12 times higher than that of epoxy. PGO nanosheets could decrease the interfacial thermal resistances of epoxy and wood microchannels, resulting in a high thermal conductivity. It is also interesting to note that the E-WPGO|| nanocomposite exhibits a higher thermal conductivity of $5.5 \text{ W m}^{-1} \text{ K}^{-1}$ —about 32 times higher than that of epoxy. The large enhancement of thermal conductivity is mainly attributed to the straighter and wider thermally conductive pathways in the E-WPGO|| nanocomposite for high-flux phonon conduction along the WPGO channel direction. Thermal stability of TMMs is very important for applications. Generally, a high temperature could increase phonon scattering and reduce the phonon path length, leading to a decreased thermal conductivity.^{17,54} Figure 7c shows the

thermal conductivity of the E-WPGO nanocomposite under high and low temperatures, and E-WPGO has good thermal stability in the temperature range from 30 to 90 °C.

To demonstrate the thermal management application of the E-WPGO nanocomposites, infrared thermal imaging tests were performed. To investigate the heat dissipation performance, pure epoxy, E-WPGO \parallel , and E-WPGO \perp nanocomposites were kept at 80 °C for 5 h, and then they were transferred to a foam stage. The corresponding temperatures are shown in Figure 7d. The E-WPGO \parallel nanocomposite exhibits a relatively fast cooling rate in comparison with pure epoxy and E-WPGO \perp . In addition, all the samples were placed on the heated stage (80 °C) to observe the heat absorption performance. It can be observed from Figure 7e that the surface temperature of the E-WPGO \parallel nanocomposite continuously increased with time at the highest rate. A model of heat conduction paths of the composite is shown in Figure 8. The heat flow transfer is along

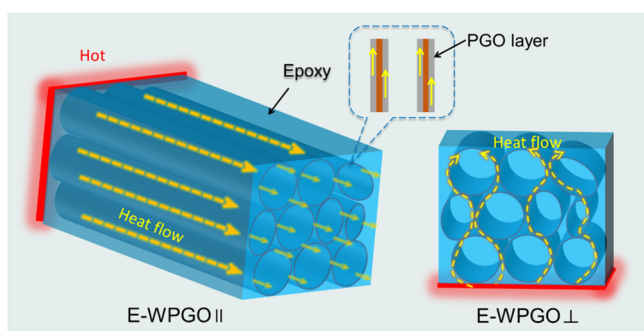


Figure 8. Schematic diagram of the proposed model for thermal conduction inside composites.

the WPGO microchannels; on the other hand, the heat flow could also occur through the PGO nanosheet to another adjacent PGO nanosheet (the arrows denote the direction of the heat flow).

For electrical and electronic applications, a reliable electrical insulation performance is very important. Figure 7f shows the volume resistivity of the pure epoxy and E-WPGO nanocomposites. The volume resistivity of pure epoxy exceeds 10^{16} Ω cm. Combining the high thermal conductivity and excellent mechanical properties, the volume electrical resistivity of E-WPGO \parallel reaches 2.6×10^{15} Ω cm, which far exceeds the critical resistivity for electrical insulation (10^9 Ω cm). The results illustrate that E-WPGO has high potential for thermal management applications.

CONCLUSIONS

In summary, we fabricated a highly aligned wood scaffold directly from natural wood via removing lignin and hemicelluloses followed by coating PGO nanosheets on the surface of wood microchannels. The wood nanocomposites (E-WPGO) featuring excellent mechanical and thermal conductivity properties were fabricated by the impregnation of the WPGO scaffolds with epoxy resin. The resulting nanocomposite possesses very high tensile stiffness, strength, and toughness due to a combination of mechanical interlocks and interfacial interactions between the epoxy resin and scaffolds. Moreover, the nanocomposite exhibits not only ultrahigh thermal conductivity but also satisfactory electrical insulation. The high-performance wood-derived polymer composites represent a promising future research direction for developing

next-generation structural thermal dissipation composites toward advanced electronic applications.

ASSOCIATED CONTENT

Supporting Information

FTIR spectra of DW, WPGO (cross section and surface), E-WPGO, uncured epoxy (EP), and cured epoxy, DSC curves of epoxy composites, and fracture surface of E-WGO and E-WPGO (PDF) The Supporting Information is available free of charge at <https://pubs.acs.org/doi/10.1021/acs.biomac.1c00786>.

(PDF)

AUTHOR INFORMATION

Corresponding Authors

Yang Wang – The Key Laboratory of Synthetic and Biological Colloids, Ministry of Education, School of Chemical and Material Engineering, Jiangnan University, Wuxi 214122, China; orcid.org/0000-0001-7875-9111; Email: ywang@jiangnan.edu.cn

Weifu Dong – The Key Laboratory of Synthetic and Biological Colloids, Ministry of Education, School of Chemical and Material Engineering, Jiangnan University, Wuxi 214122, China; orcid.org/0000-0002-7432-8362; Phone: +86-510-8532-6290; Email: wfdong@jiangnan.edu.cn

Authors

Dong Wang – The Key Laboratory of Synthetic and Biological Colloids, Ministry of Education, School of Chemical and Material Engineering, Jiangnan University, Wuxi 214122, China

Yu Zhang – The Key Laboratory of Synthetic and Biological Colloids, Ministry of Education, School of Chemical and Material Engineering, Jiangnan University, Wuxi 214122, China

Mengfei Zhang – The Key Laboratory of Synthetic and Biological Colloids, Ministry of Education, School of Chemical and Material Engineering, Jiangnan University, Wuxi 214122, China

Ting Li – The Key Laboratory of Synthetic and Biological Colloids, Ministry of Education, School of Chemical and Material Engineering, Jiangnan University, Wuxi 214122, China

Tianxi Liu – The Key Laboratory of Synthetic and Biological Colloids, Ministry of Education, School of Chemical and Material Engineering, Jiangnan University, Wuxi 214122, China

Mingqing Chen – The Key Laboratory of Synthetic and Biological Colloids, Ministry of Education, School of Chemical and Material Engineering, Jiangnan University, Wuxi 214122, China; orcid.org/0000-0002-4207-8696

Complete contact information is available at: <https://pubs.acs.org/doi/10.1021/acs.biomac.1c00786>

Notes

The authors declare no competing financial interest.

ACKNOWLEDGMENTS

This work was supported by the National Natural Science Foundation of China (22005122 and 21975108), the Natural Science Foundation of Jiangsu Province (BK20190612), the China Postdoctoral Science Foundation (2021M692158),

MOE & SAFEA, 111 Project (B13025), and the National First-Class Discipline Program of Light Industry Technology and Engineering (LITE2018-19).

REFERENCES

- (1) Lin, Y.; Chen, J.; Jiang, P.; Huang, X. Wood Annual Ring Structured Elastomer Composites with High Thermal Conduction Enhancement Efficiency. *Chem. Eng. J.* **2020**, *389*, No. 123467.
- (2) Yang, X.; Fan, S.; Li, Y.; Guo, Y.; Li, Y.; Ruan, K.; Zhang, S.; Zhang, J.; Kong, J.; Gu, J. Synchronously Improved Electromagnetic Interference Shielding and Thermal Conductivity for Epoxy Nanocomposites by Constructing 3D Copper Nanowires/thermally Annealed Graphene Aerogel Framework. *Composites, Part A* **2020**, *128*, No. 105670.
- (3) Ruan, K.; Yan, H.; Zhang, S.; Shi, X.; Guo, Y.; Gu, J. In-situ Fabrication of Hetero-structured Fillers to Significantly Enhance Thermal Conductivities of Silicone Rubber Composite Films. *Compos. Sci. Technol.* **2021**, *210*, No. 108799.
- (4) Han, Y.; Shi, X.; Yang, X.; Guo, Y.; Zhang, J.; Kong, J.; Gu, J. Enhanced Thermal Conductivities of Epoxy Nanocomposites Via Incorporating In-situ Fabricated Hetero-structured Sic-BNNS Fillers. *Compos. Sci. Technol.* **2020**, *187*, No. 107944.
- (5) Ma, T.; Zhao, Y.; Ruan, K.; Liu, X.; Zhang, J.; Guo, Y.; Yang, X.; Kong, J.; Gu, J. Highly Thermal Conductivities, Excellent Mechanical Robustness and Flexibility, and Outstanding Thermal Stabilities of Aramid Nanofiber Composite Papers with Nacre-mimetic Layered Structures. *ACS Appl. Mater. Interfaces* **2020**, *12*, 1677–1686.
- (6) Zhang, F.; Feng, Y.; Feng, W. Three-dimensional Interconnected Networks for Thermally Conductive Polymer Composites: Design, Preparation, Properties, and Mechanisms. *Mater. Sci. Eng., R* **2020**, *142*, No. 100580.
- (7) Yu, H.; Feng, Y.; Gao, L.; Chen, C.; Zhang, Z.; Feng, W. Self-healing High Strength and Thermal Conductivity of 3D Graphene/pdms Composites by the Optimization of Multiple Molecular Interactions. *Macromolecules* **2020**, *53*, 7161–7170.
- (8) Zhang, F.; Feng, Y.; Qin, M.; Gao, L.; Li, Z.; Zhao, F.; Zhang, Z.; Lv, F.; Feng, W. Composite Networks: Stress Controllability in Thermal and Electrical Conductivity of 3D Elastic Graphene-Crosslinked Carbon Nanotube Sponge/Polyimide Nanocomposite. *Adv. Funct. Mater.* **2019**, *29*, No. 1970173.
- (9) Zhang, F.; Feng, Y.; Qin, M.; Ji, T.; Lv, F.; Li, Z.; Gao, L.; Long, P.; Zhao, F.; Feng, W. Stress-sensitive Thermally Conductive Elastic Nanocomposite Based on Interconnected Graphite-welded Carbon Nanotube Sponges. *Carbon* **2019**, *145*, 378–388.
- (10) Qin, M.; Xu, Y.; Cao, R.; Feng, W.; Chen, L. Efficiently Controlling the 3D Thermal Conductivity of a Polymer Nanocomposite Via a Hyperelastic Double-continuous Network of Graphene and Sponge. *Adv. Funct. Mater.* **2018**, *28*, No. 1805053.
- (11) Guo, Y.; Ruan, K.; Shi, X.; Yang, X.; Gu, J. Factors Affecting Thermal Conductivities of the Polymers and Polymer Composites: a Review. *Compos. Sci. Technol.* **2020**, *193*, No. 108134.
- (12) Guo, Y.; Lyu, Z.; Yang, X.; Lu, Y.; Ruan, K.; Wu, Y.; Kong, J.; Gu, J. Enhanced Thermal Conductivities and Decreased Thermal Resistances of Functionalized Boron Nitride/polyimide Composites. *Composites, Part B* **2019**, *164*, 732–739.
- (13) Yang, X.; Zhu, J.; Yang, D.; Zhang, J.; Guo, Y.; Zhong, X.; Kong, J.; Gu, J. High-efficiency Improvement of Thermal Conductivities for Epoxy Composites from Synthesized Liquid Crystal Epoxy Followed by Doping BN Fillers. *Composites, Part B* **2020**, *185*, No. 107784.
- (14) Chen, J.; Huang, X.; Sun, B.; Jiang, P. Highly Thermally Conductive Yet Electrically Insulating Polymer/ Boron Nitride Nanosheets Nanocomposite Films for Improved Thermal Management Capability. *ACS Nano* **2019**, *13*, 337–345.
- (15) Chen, J.; Huang, X.; Zhu, Y.; Jiang, P. Cellulose Nanofiber Supported 3D Interconnected Bn Nanosheets for Epoxy Nanocomposites with Ultrahigh Thermal Management Capability. *Adv. Funct. Mater.* **2017**, *27*, No. 1604754.
- (16) Wang, X.; Wu, P. Highly Thermally Conductive Fluorinated Graphene Films with Superior Electrical Insulation and Mechanical Flexibility. *ACS Appl. Mater. Interfaces* **2019**, *11*, 21946–21954.
- (17) Li, M.; Liu, J.; Pan, S.; Zhang, J.; Liu, Y.; Liu, J.; Lu, H. Highly Oriented Graphite Aerogel Fabricated by Confined Liquid-Phase Expansion for Anisotropically Thermally Conductive Epoxy Composites. *ACS Appl. Mater. Interfaces* **2020**, *12*, 27476–27484.
- (18) He, D.; Wang, Y.; Song, S.; Liu, S.; Deng, Y. Significantly Enhanced Dielectric Performances and High Thermal Conductivity in Poly(vinylidene fluoride)-Based Composites Enabled by SiC@SiO₂ Core-Shell Whiskers Alignment. *ACS Appl. Mater. Interfaces* **2017**, *9*, 44839–44846.
- (19) Zhao, L.; Yan, L.; Wei, C.; Li, Q.; Huang, X.; Wang, Z.; Fu, M.; Ren, J. Synergistic Enhanced Thermal Conductivity of Epoxy Composites with Boron Nitride Nanosheets and Microspheres. *J. Phys. Chem. C* **2020**, *124*, 12723–12733.
- (20) Guo, Y.; Yang, X.; Ruan, K.; Kong, J.; Dong, M.; Zhang, J.; Gu, J.; Guo, Z. Reduced Graphene Oxide Heterostructured Silver Nanoparticles Significantly Enhanced Thermal Conductivities in Hot-Pressed Electrospun Polyimide Nanocomposites. *ACS Appl. Mater. Interfaces* **2019**, *11*, 25465–25473.
- (21) Chen, H.; Ginzburg, V. V.; Yang, J.; Yang, Y.; Liu, W.; Huang, Y.; Du, L.; Chen, B. Thermal Conductivity of Polymer-Based Composites: Fundamentals and Applications. *Prog. Polym. Sci.* **2016**, *59*, 41–85.
- (22) Vidiella del Blanco, M.; Gomez, V.; Keplinger, T.; Cabane, E.; Morales, L. F. G. Solvent-Controlled Spatial Distribution of SI-AGET-ATRP Grafted Polymers in Lignocellulosic Materials. *Biomacromolecules* **2019**, *20*, 336–346.
- (23) Guan, Q. F.; Han, Z. M.; Ling, Z. C.; Yang, H. B.; Yu, S. H. Sustainable Wood-Based Hierarchical Solar Steam Generator: A Biomimetic Design with Reduced Vaporization Enthalpy of Water. *Nano Lett.* **2020**, *20*, 5699–5704.
- (24) Chen, Y.; Fu, J.; Dang, B.; Sun, Q.; Li, H.; Zhai, T. Artificial Wooden Nacre: A High Specific Strength Engineering Material. *ACS Nano* **2020**, *14*, 2036–2043.
- (25) Li, T.; Chen, C.; Brozena, A. H.; Zhu, J. Y.; Xu, L.; Driemeier, C.; Dai, J.; Rojas, O. J.; Isogai, A.; Wågberg, L.; Hu, L. Developing Fibrillated Cellulose as A Sustainable Technological Material. *Nature* **2021**, *590*, 47–56.
- (26) Berglund, L. A.; Burgert, I. Bioinspired Wood Nanotechnology for Functional Materials. *Adv. Mater.* **2018**, *30*, No. 1704285.
- (27) Li, T.; Zhai, Y.; He, S.; Gan, W.; Hu, L. A radiative cooling structural material. *Science* **2019**, *364*, 760–763.
- (28) Frey, M.; Schneider, L.; Masania, K.; Keplinger, T.; Burgert, I. Delignified Wood–Polymer Interpenetrating Composites Exceeding the Rule of Mixtures. *ACS Appl. Mater. Interfaces* **2019**, *11*, 35305–35311.
- (29) Guo, H.; Warnicke, P.; Griffa, M.; Müller, U.; Chen, Z.; Schaeublin, R.; Zhang, Z.; Luković, M. Hierarchical Porous Wood Cellulose Scaffold with Atomically Dispersed Pt Catalysts for Low-Temperature Ethylene Decomposition. *ACS Nano* **2019**, *13*, 14337–14347.
- (30) Jia, C.; Chen, C.; Mi, R.; Li, T.; Dai, J.; Yang, Z.; Pei, Y.; He, S.; Bian, H.; Jang, S. H.; Zhu, J. Y.; Yang, B.; Hu, L. Clear Wood toward High-Performance Building Materials. *ACS Nano* **2019**, *13*, 9993–10001.
- (31) Guan, H.; Cheng, Z.; Wang, X. Highly Compressible Wood Sponges with a Spring-like Lamellar Structure as Effective and Reusable Oil Absorbents. *ACS Nano* **2018**, *12*, 10365–10373.
- (32) Zhu, H.; Luo, W.; Ciesielski, P. N.; Fang, Z.; Zhu, J. Y.; Henriksson, G.; Himmel, M. E.; Hu, L. Wood-Derived Materials for Green Electronics, Biological Devices, and Energy Applications. *Chem. Rev.* **2016**, *116*, 9305–9374.
- (33) Gan, W.; Chen, C.; Giroux, M.; Zhong, G.; Goyal, M. M.; Wang, Y.; Ping, W.; Song, J.; Xu, S.; He, S.; Jiao, M.; Wang, C.; Hu, L. Conductive Wood for High-Performance Structural Electromagnetic Interference Shielding. *Chem. Mater.* **2020**, *32*, 5280–5289.

- (34) Yang, J.; Chen, Y.; Jia, X.; Li, Y.; Wang, S.; Song, H. Wood-Based Solar Interface Evaporation Device with Self-Desalting and High Antibacterial Activity for Efficient Solar Steam Generation. *ACS Appl. Mater. Interfaces* **2020**, *12*, 47029–47037.
- (35) Liang, C.; Qiu, H.; Song, P.; Shi, X.; Kong, J.; Gu, J. Ultra-light MXene Aerogel/Wood-derived Porous Carbon Composites with Wall-like “Mortar/Brick” Structures for Electromagnetic Interference Shielding. *Sci. Bull.* **2020**, *65*, 616–622.
- (36) Zhu, M.; Song, J.; Li, T.; Gong, A.; Wang, Y.; Dai, J.; Yao, Y.; Luo, W.; Henderson, D.; Hu, L. Highly Anisotropic, Highly Transparent Wood Composites. *Adv. Mater.* **2016**, *28*, 5181–5187.
- (37) Li, Y.; Yang, X.; Fu, Q.; Rojas, R.; Yan, M.; Berglund, L. Towards Centimeter Thick Transparent Wood Through Interface Manipulation. *J. Mater. Chem. A* **2018**, *6*, 1094–1101.
- (38) Li, T.; Song, J.; Zhao, X.; Yang, Z.; Pastel, G.; Xu, S.; Jia, C.; Dai, J.; Chen, C.; Gong, A. Anisotropic, Lightweight, Strong, and Super Thermally Insulating Nanowood with Naturally Aligned Nanocellulose. *Sci. Adv.* **2018**, *4*, No. eaar3724.
- (39) Lee, H.; Dellatore, S. M.; Miller, W. M.; Messersmith, P. B. Mussel-Inspired Surface Chemistry for Multifunctional Coatings. *Science* **2007**, *318*, 426–430.
- (40) Xu, L. Q.; Yang, W. J.; Neoh, K. G.; Kang, E. T.; Fu, G. D. Dopamine-Induced Reduction and Functionalization of Graphene Oxide Nanosheets. *Macromolecules* **2010**, *43*, 8336–8339.
- (41) Yuan, H.; Wang, Y.; Li, T.; Wang, Y.; Ma, P.; Zhang, H.; Yang, W.; Chen, M.; Dong, W. Fabrication of Thermally Conductive and Electrically Insulating Polymer Composites with Isotropic Thermal Conductivity by Constructing a Three-dimensional Interconnected Network. *Nanoscale* **2019**, *11*, 11360–11368.
- (42) Wang, Y.; Zhang, Z.; Li, T.; Ma, P.; Zhang, X.; Xia, B.; Chen, M.; Du, M.; Liu, T.; Dong, W. Artificial Nacre Epoxy Nanomaterials Based on Janus Graphene Oxide for Thermal Management Applications. *ACS Appl. Mater. Interfaces* **2020**, *12*, 44273–44280.
- (43) Yuan, H.; Wang, Y.; Li, T.; Ma, P.; Zhang, S.; Du, M.; Chen, M.; Dong, W.; Ming, W. Highly Thermal Conductive and Electrically Insulating Polymer Composites Based on Polydopamine-coated Copper Nanowire. *Compos. Sci. Technol.* **2018**, *164*, 153–159.
- (44) Lian, M.; Fan, J.; Shi, Z.; Zhang, S.; Li, H.; Yin, J. Gelatin-assisted Fabrication of Graphene-based Nacre with High Strength, Toughness, and Electrical Conductivity. *Carbon* **2015**, *89*, 279–289.
- (45) Zhang, H.; Peng, C.; Yang, J.; Lv, M.; Liu, R.; He, D.; Fan, C.; Huang, Q. Uniform Ultrasmall Graphene Oxide Nanosheets with Low Cytotoxicity and High Cellular Uptake. *ACS Appl. Mater. Interfaces* **2013**, *5*, 1761–1767.
- (46) Wang, Y.; Li, T.; Ma, P.; Zhang, S.; Zhang, H.; Du, M.; Xie, Y.; Chen, M.; Dong, W.; Ming, W. Artificial Nacre from Supramolecular Assembly of Graphene Oxide. *ACS Nano* **2018**, *12*, 6228–6235.
- (47) Wang, Y.; Yuan, H.; Ma, P.; Bai, H.; Chen, M.; Dong, W.; Xie, Y.; Deshmukh, Y. S. Superior Performance of Artificial Nacre Based on Graphene Oxide Nanosheets. *ACS Appl. Mater. Interfaces* **2017**, *9*, 4215–4222.
- (48) Wang, S.; Li, K.; Zhou, Q. High Strength and Low Swelling Composite Hydrogels from Gelatin and Delignified Wood. *Sci. Rep.* **2020**, *10*, 17842.
- (49) Zangmeister, R. A.; Morris, T. A.; Tarlov, M. J. Characterization of Polydopamine Thin Films Deposited at Short Times by Autoxidation of Dopamine. *Langmuir* **2013**, *29*, 8619–8628.
- (50) Chen, S.; Cao, Y.; Feng, J. Polydopamine As an Efficient and Robust Platform to Functionalize Carbon Fiber for High-Performance Polymer Composites. *ACS Appl. Mater. Interfaces* **2014**, *6*, 349–356.
- (51) Yang, L.; Phua, S. L.; Teo, J. K. H.; Toh, C. L.; Lau, S. K.; Ma, J.; Lu, X. A Biomimetic Approach to Enhancing Interfacial Interactions: Polydopamine-Coated Clay as Reinforcement for Epoxy Resin. *ACS Appl. Mater. Interfaces* **2011**, *3*, 3026–3032.
- (52) Subramanian, A. S.; Tey, J. N.; Zhang, L.; Ng, B. H.; Roy, S.; Wei, J.; Hu, X. M. Synergistic Bond Strengthening in Epoxy Adhesives Using Polydopamine /MWCNT Hybrids. *Polymer* **2016**, *82*, 285–294.
- (53) Fredi, G.; Simon, F.; Sychev, D.; Melnyk, I.; Janke, A.; Scheffler, C.; Zimmerer, C. Bioinspired Polydopamine Coating as an Adhesion Enhancer Between Paraffin Microcapsules and an Epoxy Matrix. *ACS Omega* **2020**, *5*, 19639–19653.
- (54) Chen, S.; Wu, Q.; Mishra, C.; Kang, J.; Zhang, H.; Cho, K.; Cai, W.; Balandin, A. A.; Ruoff, R. S. Thermal conductivity of isotopically modified graphene. *Nat. Mater.* **2012**, *11*, 203–207.